The fracture characteristics of a superplastic single phase copper alloy

SHEN-ANN SHEI*, TERENCE G. LANGDON
Department of Materials Science, University of Southern California, Los Angeles, California 90007, USA

A superplastic single phase copper alloy exhibits a sigmoidal relationship between strain rate and stress at 823 K, dividing the behaviour into three regions. Maximum elongation to fracture (~380%) occurs at intermediate strain rates at the lower end of region II, and there is a decrease in total elongation at both low (region I) and high (region III) strain rates. No necking is observed in regions I and II, and there is only very slight necking in region III. Internal cavities are formed at all strain rates, but the appearance of the cavities depends critically on the imposed strain rate. At high strain rates, the cavities are small and lie in strings parallel to the tensile axis; but as the strain rate is reduced the cavities become larger, more rounded, and essentially randomly distributed. The mode of failure is ductile rupture in region III, but void growth and interlinkage become increasingly important with decreasing strain rate.

1. Introduction

In early investigations of superplasticity in metals, it was generally assumed that internal cavities were not formed during superplastic flow [1]. More recently, however, the importance of void formation in superplasticity has been very firmly established, at least for some materials, by metallographic studies on several Cu alloys [2–15], various steels [13–19], Al–Mg [20] and Al–Zn–Mg [21] alloys, the Al–Al₂Cu eutectic [22], the Zn–22% Al eutectoid [23], and ternary alloys of the Pb–Sn eutectic containing 4 wt % Cu [15], 4 wt % Sb [15], or 5.6 wt % Ag [24].

With only one exception [6], all of the results reported to date have been concerned with fracture behaviour under rather limited conditions of stress and strain rate, and there has been no systematic study of the fracture characteristics over a very wide range of strain rates at a single temperature. This is a serious omission, because it prevents any detailed conclusions concerning the fracture behaviour in the three regions of plastic flow generally associated with superplastic materials. Unfortunately, in the only investigation in which the internal microstructures were examined after failure at different strain rates at a constant temperature, the results were not generally representative because grain growth of up to an order of magnitude occurred at the lowest strain rates [6].

The present work was undertaken to provide detailed information on the influence of strain rate on the fracture characteristics of a superplastic material, by examining the microstructures and fracture surfaces of specimens tested to failure at a constant temperature over four orders of magnitude of strain rate. A commercial copper base alloy was selected for this purpose for two reasons: (i) it had already been demonstrated that this alloy was superplastic and exhibited extensive cavitation [4, 9, 11, 25, 26], and (ii) the mechanical properties of this material were established in a detailed investigation conducted earlier [27].

2. Experimental procedure

Experiments were performed on Coronze CDA 638, a commercial alloy containing 95 wt % Cu, 2.8 wt % Al, 1.8 wt % Si, and 0.4 wt % Co. This alloy is essentially single phase up to a temperature

---

of 1273 K, but contains a uniform dispersion of a Co-rich phase which inhibits grain growth and thus facilitates the production of the very small and stable grain sizes required for superplastic deformation.

The material was received in the form of hot-rolled sheets, 1.3 mm in thickness, which had been thermomechanically treated to give an average spatial grain diameter, d (defined as $1.74 \times \bar{L}$, where $\bar{L}$ is the mean linear intercept), of $3.0\,\mu m$.

Tensile specimens, having a gauge length of 2.54 cm, were machined from the sheets with the tensile axis parallel to the rolling direction. The specimens were tested on an Instron machine operating at a constant rate of cross-head displacement. The strain rates quoted herein refer to the initial strain rates experienced by each specimen, calculated from the initial gauge length. All tests were conducted in air at a temperature of 823 K.

Initially, tests were performed to determine the relationship between strain rate and steady-state stress using a strain rate cycling technique. For these experiments, the total strain of each specimen was never greater than 8%, because there was a tendency for the maximum flow stress to decrease at higher strains. To obtain accurate results at the highest strain rates, each of the specimens used for these datum points was tested at a single strain rate. The temperature was obtained using a three-zone split vertical furnace and a proportional temperature controller. A continuous monitor of the specimen temperature during each test showed that the variation in temperature was less than ± 1 K of the selected value.

Having established the strain rate: stress relationship at 823 K, tests were performed in which individual specimens were pulled to fracture at a single rate of cross-head displacement. The displacements used for these tests were equivalent to initial strain rates in the range from 8.33×10^{-6} to 3.33×10^{-2} sec^{-1}. A single zone split vertical furnace, 61 cm in length, was used to maintain a constant temperature over the entire gauge length during each test, and the temperature variation along the specimen was monitored continuously by placing thermocouples at either end of the gauge length prior to testing. These measurements showed that the temperature was maintained to within 823 ± 5 K for engineering strains up to a maximum of 380%.

After fracture, all specimens were carefully sectioned along the gauge length and mechanically polished for examination by optical microscopy. In addition, the surfaces at the point of fracture were examined using a scanning electron microscope.

3. Experimental results
3.1. Relationship between strain rate and stress

The relationship between the imposed tensile strain rate, $\dot{\epsilon}$, and the measured steady-state stress, σ, is shown in Fig. 1, covering four orders of magnitude of imposed strain rate. The results show the sigmoidal behaviour characteristic of superplastic metals.

At low strain rates (region I, $\dot{\epsilon} \leqslant 3.33 \times 10^{-4}$ sec^{-1}), the stress exponent, n ($= (\partial \ln \dot{\epsilon}/\partial \ln \sigma)$), is high ($\sim 4.6$); whereas over a rather narrow intermediate range of strain rates (region II, 3.33×10^{-4} sec$^{-1} < \dot{\epsilon} < 8.33 \times 10^{-4}$ sec^{-1}), there is a lower value of $n (\sim 2.8)$; and at high strain rates (region III, $\dot{\epsilon} \geqslant 8.33 \times 10^{-4}$ sec^{-1}), the value of n is again high (~ 4.7). The results shown in Fig. 1 are very similar to those reported for other superplastic materials (for example, Zn—22% Al [28]). A more detailed description of the mechanical characteristics of this alloy is given elsewhere [27].
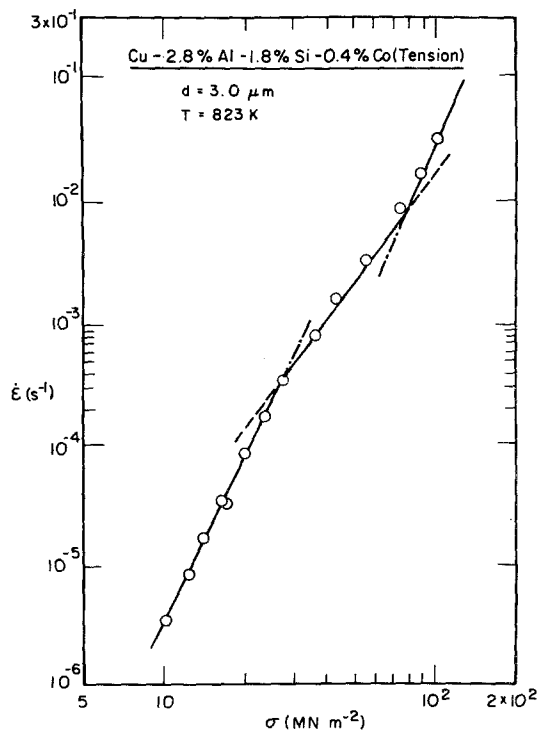

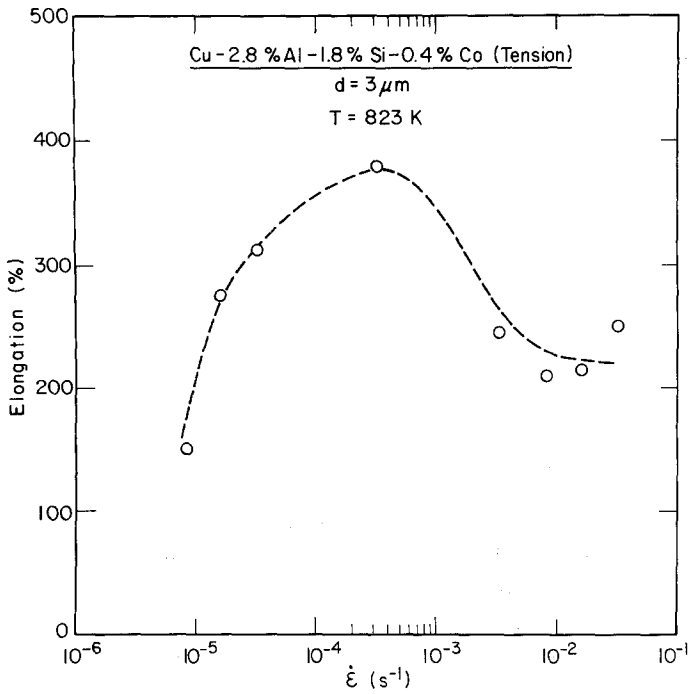*Figure 1* Strain rate versus stress for a grain size of $3.0\,\mu m$ and a temperature of 823 K.

Figure 2 Elongation at fracture as a percentage versus initial strain rate for an initial grain size of $3.0\,\mu m$ and a temperature of 823 K.

3.2. Variation of elongation with strain rate

Individual specimens were tested to failure at initial strain rates from 8.33×10^{-6} to 3.33×10^{-2} sec^{-1}. The results of these ductility tests are shown in Fig. 2, where the elongation at fracture is defined as $(L_f - L_0)/L_0\%$ where L_f is the final gauge length of the specimen at the point of fracture and L_0 is the original gauge length prior to testing.

Although there is some scatter in the individual datum points given in Fig. 2, a comparison with Fig. 1 shows that the maximum elongation occurs at a strain rate which is at the lower end of region II, and the elongation at fracture decreases in
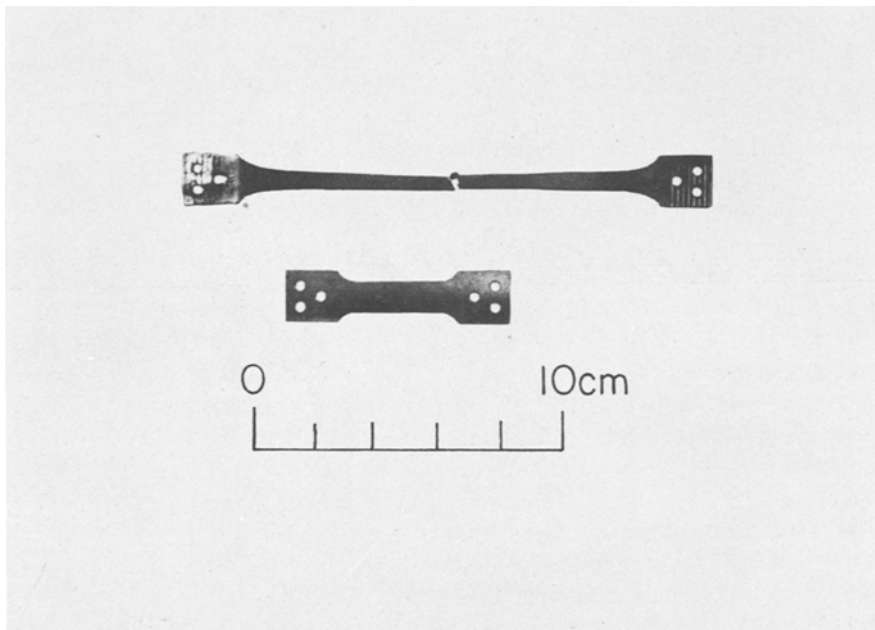

Figure 3 Tensile specimen deformed to failure at an initial strain rate of 3.33×10^{-4} sec^{-1} (upper); untested tensile specimen (lower).
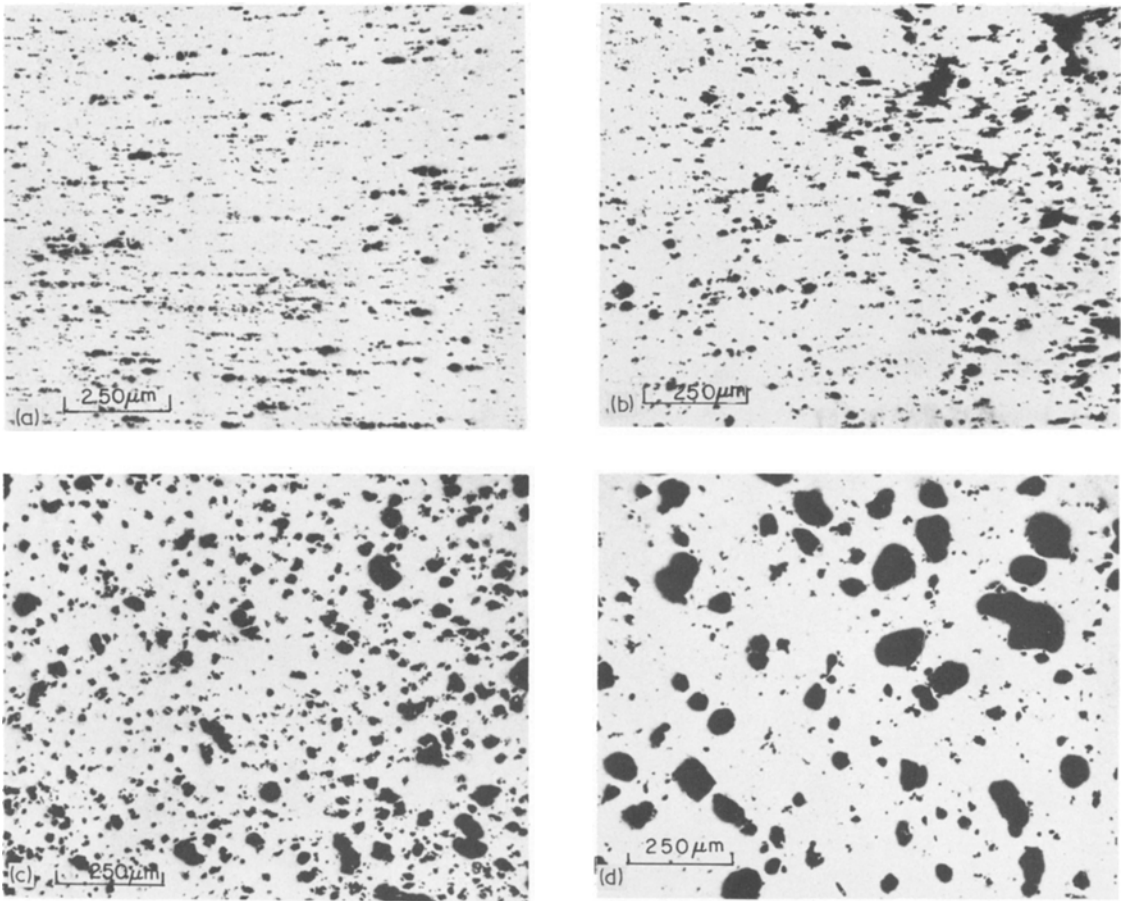
Figure 4 Optical photomicrographs of typical areas in the gauge section of specimens pulled to fracture at initial strain rates of (a) 3.33×10^{-2} sec^{-1}, (b) 8.33×10^{-3} sec^{-1}, (c) 3.33×10^{-4} sec^{-1}, and (d) 1.67×10^{-5} sec^{-1}. The tensile axis is horizontal.

regions I and III. No necking was observed in any of the specimens tested at the lower strain rates; this is indicated in Fig. 3 by the uniform deformation exhibited by the specimen tested at $\dot{\epsilon} = 3.33 \times 10^{-4}$ sec^{-1}, corresponding to the maximum elongation of 380%. Slight necking was visible in the specimens tested at the three highest strain rates (in region III), but the total extent of necking was always very small.

3.3. Dependence of cavity formation on strain rate

Internal cavitation was observed in the gauge sections of all of the specimens after fracture, but the appearance of the cavities depended very markedly on the imposed strain rate.

Fig. 4 shows representative optical photomicrographs of typical areas in the gauge section of specimens pulled to fracture at initial strain rates of

(a) 3.33×10^{-2} sec^{-1} (region III), (b) 8.33×10^{-3} sec^{-1} (region II/III transition), (c) 3.33×10^{-4} sec^{-1} (region I/II transition), and (d) 1.67×10^{-5} sec^{-1} (region I). In each case, the tensile axis is horizontal.

At very high strain rates in region III (Fig. 4a), the cavities are generally small, there are few examples of interlinkage, and the cavities tend to lie in strings which are parallel to the tensile axis. The tendency to form strings of this type was noted earlier for a microduplex steel [16] and the Zn−22%Al eutectoid [23]. At the transition between regions II and III (Fig. 4b), the cavities are larger and more randomly distributed, although there is again some alignment along the tensile axis. Several of the larger cavities have a rather ragged appearance at this strain rate, indicative of the very short time available for growth by a diffusion process.

At the transition between regions I and II (Fig. 4c), which corresponded to the point of maximum elongation, the cavities are large, reasonably uniform in size, and essentially randomly distributed throughout the gauge section. At even lower strain rates (Fig. 4d), corresponding to very slow deformation in region I, some very large and rounded cavities are visible, and there is no tendency for any preferred alignment.

3.4. Appearance of the fracture surfaces

Fig. 5 shows the fracture surfaces of the four specimens selected for Fig. 4, indicating that the final mode of fracture depends also on the imposed strain rate.

For the specimen tested in region III (Fig. 5a), many tiny holes are visible on the fracture surface, there are numerous fairly sharp ridges, and it is clear that final fracture occurred by a process of
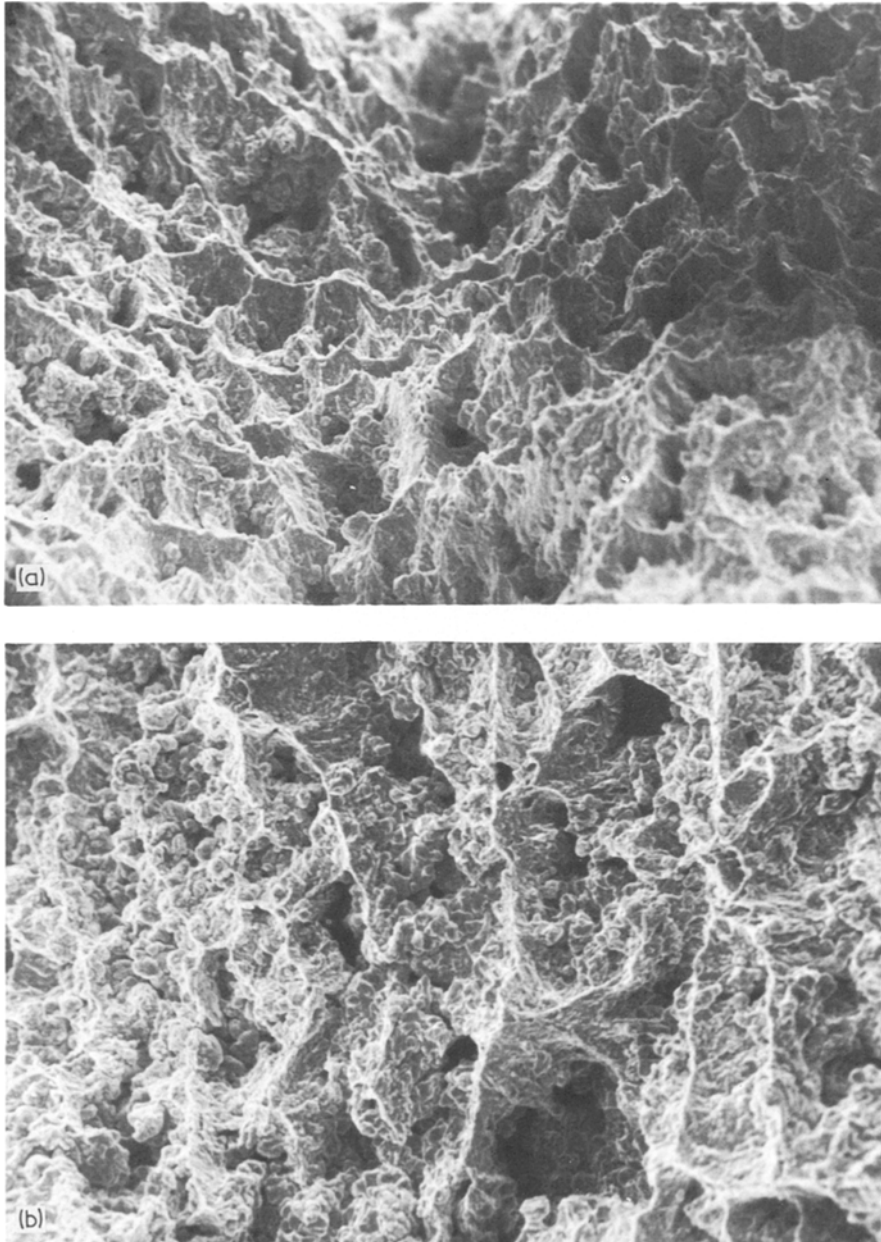

Figure 5 Scanning electron micrographs of the fracture surfaces of specimens pulled to fracture at inital strain rates of (a) $3.33 \times 10^{-2} \, \text{sec}^{-1}$, (b) $8.33 \times 10^{-3} \, \text{sec}^{-1}$, (c) $3.33 \times 10^{-4} \, \text{sec}^{-1}$, and (d) $1.67 \times 10^{-5} \, \text{sec}^{-1}$. Magnification: $\times 1000$.

ductile rupture. The individual grains are visible on this fracture surface in only a few isolated places. At the transition between regions II and III (Fig. 5b), the individual grains are generally visible over the entire surface, but there are also several prominent ridges, and the final fracture mode was again a ductile tearing process. At the transition between regions I and II (Fig. 5c), the individual grains are very clearly visible, there are no obvious ridges, and there is an indication of some void growth and interlinkage at the fracture surface. Finally, at the very low strain rates in region I (Fig. 5d), large holes are visible on the fracture surface, and failure was apparently initiated by void interlinkage. This surface also reveals evidence for some grain growth due to the long-term nature of the test.
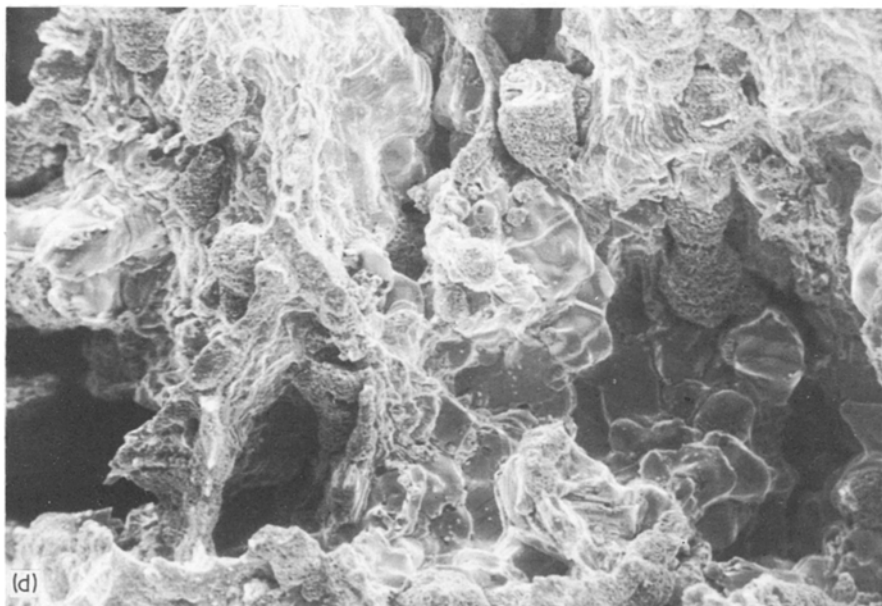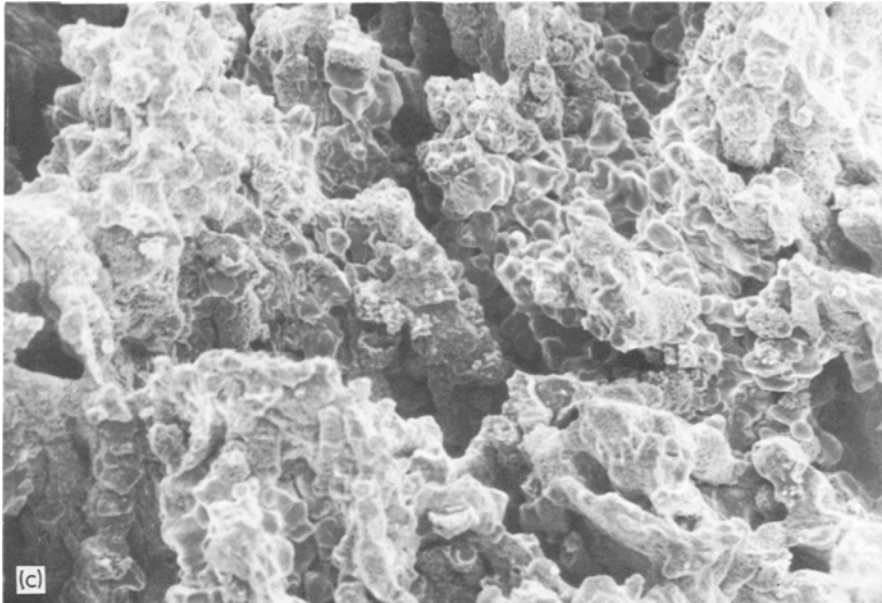

Figure 5 continued.

4. Discussion

4.1. Mechanical properties and elongation to failure

The sigmoidal relationship depicted in Fig. 1 is very similar to the results obtained earlier for two other superplastic materials, Pb–62% Sn [29] and Zn–22% Al [28]. The major differences between these materials are the values of the stress exponent, n, in regions I and II. For the Cu alloy, $n \simeq 2.8$ in region II, whereas the equivalent values for Pb–62% Sn and Zn–22% Al are ~1.65 [29] and ~2.25 [28], respectively. Similarly, the value of n is ~4.6 in region I in the present investigation, which is significantly higher than the values of ~3.0 for Pb–62% Sn [29] and ~4.1 for Zn–22% Al [28].

It is well known that the total ductility depends, at least in part, on the value of n, since necks within the gauge length become diffuse and fail to propagate as n decreases to 1. This may be demonstrated by combining the expressions for $\sigma (= P/A$, where P is the tensile force and A is the cross-sectional area), $\dot{\epsilon}(= -(1/A) \, \mathrm{d}A/\mathrm{d}t$, where t is the time), and the general creep equation ($\dot{\epsilon} = B\sigma^n$, where B is a constant), to give

$$-\mathrm{d}A/\mathrm{d}t \; = \; BP^n A^{1-n} \qquad (1)$$

Equation 1 shows that $\mathrm{d}A/\mathrm{d}t$ approaches a common level which is independent of A as $n \rightarrow 1$, so that failure by necking becomes increasingly less important at lower values of n.

A comparison of the values of n obtained in the present investigation and in Pb–62% Sn and Zn–22% Al leads to two important predictions:

(i) The Cu alloy is expected to exhibit significantly lower elongations to failure because of the higher stress exponents. This prediction is confirmed by the experimental results, since the maximum elongation of 380% obtained in the present work at the lower end of region II contrasts with elongations of up to 4850% in Pb–62% Sn [30] and up to 2900% in Zn–22% Al [31, 32].

(ii) The Cu alloy is expected to exhibit significant necking in region I because $n \simeq 4.6$. This prediction is *not* confirmed by the experiments, since no necking was apparent in the Cu alloy after failure at ~200 to 300% elongation at the lowest strain rates. By contrast, it was noted earlier that specimens of Zn–22% Al, which failed at elongations of ~400% under comparable strain rates in region I, showed very clear evidence for neck formation within the gauge section [32, 33].

This apparent dichotomy arises because Equation 1 relates strictly to conditions of constant volume, and thus it fails to incorporate the influence of cavitation on the fracture process. This is a serious omission for materials such as Cu alloys, where cavity formation is generally fairly prevalent.

The shape of the curve in Fig. 2, in which the elongation reaches a maximum at intermediate strain rates and decreases at both very rapid and very slow strain rates, is similar to results reported earlier for various Cu alloys [5, 6, 34] and Zn–22% Al [31, 32]. In addition, the total elongations documented in this work are comparable to some isolated values reported in other investigations on the same material. For example, an elongation of 318% was obtained for a grain size of 1 μm and a strain rate of 6.5×10^{-4} sec^{-1} at 823 K [9], and this is in close agreement with the data for a grain size of 3 μm shown in Fig. 2.

4.2. Fracture characteristics

Several of the results obtained in this investigation support those reported for the superplastic Cu–40% Zn alloy [6]. In both materials, the cavities were present throughout the gauge lengths of the fractured specimens, and larger cavities were observed after fracture at the lower strain rates. Observations on the Cu–40% Zn alloy suggested that the cavities do not readily interlink, and this is supported by an examination of the photomicrographs of the present alloy. For example, Figs. 4a and b clearly show several instances where there are thin ligaments of material between adjacent cavities, thereby indicating that an important feature of the fracture process is probably the resistance to cavity interlinkage by internal necking of these ligaments.

There is one important difference between these results and those obtained on Cu–40% Zn [6]. The latter alloy revealed very few cavities after fracture at the lowest strain rate, and this contrasts with the present investigation where the cavities were large and numerous under these conditions (Fig. 4d). This difference probably arises because of the occurrence of grain growth by up to an order of magnitude in Cu–40% Zn, so that stress concentrations, which may give rise to grain boundary cavities, are very readily removed by boundary migration. In this work, a comparison of Figs. 5a and d indicates that the grain size increased at the lower strain rate by a factor of ~5. The present observation of an increase in cavitation with a

decrease in strain rate is similar to the conclusions obtained from density measurements on microduplex steels [16, 18].

Although no measurements were taken to determine the area fraction of cavities in the gauge section after failure, the photomicrographs in Fig. 4 suggest that maximum cavitation is associated with maximum elongation (Fig. 4c). This is consistent with quantitative measurements reported for Al–5% Mg alloys [20], but it contrasts with qualitative observations on the Zn–22% Al eutectoid [23] where cavitation was more extensive after low strains to failure in region I.

A significant feature of Fig. 4 is the formation of cavity strings parallel to the tensile axis at the faster strain rates. After the nucleation of a cavity, growth may occur either by vacancy condensation or through a deformation process due to the applied stress. Calculations show that the latter process is favoured at low values of $\sigma/\dot{\epsilon}$ and this gives rise to cavities which are elongated in the direction of the tensile stress [35]. The photomicrographs in Fig. 4 are consistent with these calculations, because there is a significantly lower value of $\sigma/\dot{\epsilon}$ in region III ($\sim 10^4$ MNsec m^{-2}) than in region I ($\sim 10^6$ MNsec m^{-2}).

It is also interesting to note that the two specimens shown in Figs. 4a and d exhibited almost identical elongations to fracture (250% and 275%, respectively), but there is no similarity in the appearance of cavitation within the two gauge sections. At the very high strain rate, there are many cavity nuclei but the short time to failure ($\sim 1\frac{1}{4}$ min) prevents any appreciable cavity growth (Fig. 4a). By contrast, sufficient time is available at the low strain rate (~ 45 h) for considerable cavity growth by vacancy diffusion, thereby giving the rounded cavities shown in Fig. 4d.

The scanning micrographs of the fracture surfaces shown in Fig. 5 are consistent with the cavitation studies presented in Fig. 4, and it is clear that cavity nucleation plays an important role under all experimental conditions employed in this work. By using 1 MV electron microscopy [25], it has been demonstrated that cavities are nucleated in this alloy at 873 K by the action of grain boundary sliding which opens up voids on one side of precipitate particles lying in the grain boundaries. At high strain rates, as in Figs. 4a and 5a, cavities grow under the action of the applied stress, and thereby decrease the cross-sectional area of the specimen. Void interlinkage is then dependent on the fracture of internal ligaments, and, as shown in Fig. 5a, failure ultimately occurs by a ductile rupture process. A similar sequence is also visible in Figs. 4b and 5b.

At the strain rate corresponding to maximum elongation, shown in Fig. 5c, grain boundary sliding is an important deformation process so that the grains are clearly visible on the fracture surface. This gives rise to a very large number of internal cavities, essentially uniformly distributed, which appear to grow and interlink by both diffusion and deformation processes. Failure occurs because, although there is no visible external necking, the high degree of internal cavitation, including some interlinkage, very much reduces the effective cross-sectional area.

The low strain rates associated with region I (Fig. 5d) lead to the nucleation of fewer cavities, and their subsequent growth by vacancy diffusion. Final fracture is again a consequence of void interlinkage, but, under these conditions, very large and stable holes exist in the gauge length of the specimen at failure (Fig. 4d).

5. Summary and conclusions

(1) A superplastic single phase Cu alloy containing a dispersed Co-rich phase exhibits a sigmoidal relationship between the imposed tensile strain rate and the steady-state stress when tested with a grain size of 3.0μm and at a temperature of 823 K. The stress exponent is ~ 4.6 at low strain rates (region I), ~ 2.8 at intermediate strain rates (region II), and ~ 4.7 at high strain rates (region III).

(2) Maximum elongation to fracture ($\sim 380\%$) occurs at the lower end of region II, and there is a decrease in the total elongation in regions I and III. No necking occurs in regions I and II, and there is only very slight necking in region III.

(3) Internal cavities are formed throughout the gauge section at all strain rates, but the appearance of the cavities depends critically on the imposed strain rate. At high strain rates (region III), the cavities are small and tend to lie in strings parallel to the tensile axis. As the strain rate is decreased to region II, the cavities become larger and more randomly distributed. At much lower strain rates (region I), the cavities are large and rounded, and there is essentially a random distribution.

(4) Examination of the fracture surfaces shows that failure occurs by ductile rupture in region III, but void growth and interlinkage become increasingly important with decreasing strain rate.

References

1. R. H. JOHNSON, *Met. Rev.* **15** (1970) 115.
2. D. M. R. TAPLIN, G. L. DUNLOP, S. SAGAT and R. H. JOHNSON, "Proceedings of the 2nd Interamerican Conference on Materials Technology" Vol. I (American Society of Mechanical Engineers, New York, 1970) p. 253.
3. G. L. DUNLOP, J.D. REID and D.M.R. TAPLIN, *Met. Trans.* **2** (1971) 2308.
4. R. G. FLECK and D. M. R. TAPLIN, *Can Met. Quart.* **11** (1972) 299.
5. D. M. R. TAPLIN and S. SAGAT, *Mater. Sci. Eng.* **9** (1972) 53.
6. S. SAGAT, P. BLENKINSOP and D. M. R. TAPLIN, *J. Inst. Metals* **100** (1972) 268.
7. R. D. SCHELLENG and G. H. REYNOLDS, *Met. Trans.* **4** (1973) 2199.
8. G. L. DUNLOP, E. SHAPIRO, D. M. R. TAPLIN and J. CRANE, *ibid* **4** (1973) 2039.
9. R. G. FLECK, C. J. BEEVERS and D. M. R. TAPLIN, *J. Mater. Sci.* **9** (1974) 1737.
10. T. CHANDRA, J. J. JONAS and D. M. R. TAPLIN, *J. Australian Inst. Metals* **20** (1975) 220.
11. R. G. FLECK, C. J. BEEVERS and D. M. R. TAPLIN, *Met. Sci.* **9** (1975) 49.
12. S. SAGAT and D. M. R. TAPLIN, *Acta Met.* **24** (1976) 307.
13. N. RIDLEY, C. W. HUMPHRIES and D. LIVESEY, "Proceedings of the 4th International Conference on the Strength of Metals and Alloys" Vol. 1 (Laboratoire de Physique du Solide, E.N.S.M.I.M., Nancy, France, 1976) p. 433.
14. N. RIDLEY and C. W. HUMPHRIES, "Grain Boundaries" (The Institution of Metallurgists, London, 1976) p. E29.
15. N. RIDLEY and D. W. LIVESEY, "Fracture 1977," Vol. 2, edited by D. M. R. Taplin (University of Waterloo Press, Waterloo, Ontario, 1977) p. 533.
16. C. W. HUMPHRIES and N. RIDLEY, *J. Mater. Sci.* **9** (1974) 1429.
17. C. I. SMITH, B. NORGATE and N. RIDLEY, *Met. Sci.* **10** (1976) 182.
18. C. I. SMITH, B. NORGATE and N. RIDLEY, *Met. Sci.* **10** (1976) 182.
19. M. J. STEWART, *Met. Trans. A* **7A** (1976) 399.
20. D. M. R. TAPLIN and R. F. SMITH, "Fracture 1977," Vol. 2, edited by D. M. R. Taplin (University of Waterloo Press, Waterloo, Ontario, 1977) p. 541.
21. K. MATUKI and M. YAMADA, *J. Japan Inst. Metals* **37** (1973) 448.
22. M. W. A. BRIGHT, D. M. R. TAPLIN and H. W. KERR, *J. Eng. Mater. Technol.* **97** (1975) 1.
23. H. ISHIKAWA, D. G. BHAT, F. A. MOHAMED and T. G. LANGDON, *Met. Trans. A* **8A** (1977) 523.
24. C. W. HUMPHRIES and N. RIDLEY, *J. Mater. Sci.* **12** (1977) 851.
25. R. G. FLECK, D. M. R. TAPLIN and C. J. BEEVERS, *Acta Met.* **23** (1975) 415.
26. R. G. FLECK, C. J. BEEVERS and D. M. R. TAPLIN, *Met. Sci.* **10** (1976) 413.
27. S. -A. SHEI and T. G. LANGDON, *Acta Met.* (in press).
28. F. A. MOHAMED and T. G. LANGDON, *ibid* **23** (1975) 117.
29. *Idem, Phil. Mag.* **32** (1975) 697.
30. M. M. I. AHMED and T. G. LANGDON, *Met. Trans. A* **8A** (1977) 1832.
31. H. ISHIKAWA, F. A. MOHAMED and T. G. LANGDON, *Phil. Mag.* **32** (1975) 1269.
32. F. A. MOHAMED, M. M. I. AHMED and T. G. LANGDON, *Met. Trans. A* **8A** (1977) 933.
33. T. G. LANGDON and F. A. MOHAMED, "Fracture 1977," Vol. 2, edited by D. M. R. Taplin (University of Waterloo Press, Waterloo, Ontario, 1977) p. 525.
34. G. L. DUNLOP and D. M. R. TAPLIN, *J. Mater. Sci.* **7** (1972) 84.
35. J. W. HANCOCK, *Met. Sci.* **10** (1976) 319.